Received: 24 October 2018 | Revised: 26 December 2018 | Accepted: 15 January 2019

DOI: 10.1002/pat.4562

RESEARC HARTICLE

WILEY polymers advanced technologies

Synthesis and photovoltaic investigation of dithieno[2,3-*d*:2′,3′-*d*′]-benzo[1,2-*b*:3,4-*b*′:5,6-*d*″]trithiophene-based conjugated polymer with an enlarged π-conjugated system

Xiaofang Zhang[1] | **Minjing Zhang**[1] | **Junfeng Tong**[1,2] | **Pengzhi Guo**[3] | **Xunchang Wang**[4] | **Zezhou Liang**[1] | **Yufei Wang**[1] | **Yangjun Xia**[1,2]

[1] Key Laboratory of Optoelectronic Technology and Intelligent Control of Ministry Education, Lanzhou Jiaotong University, Lanzhou, PR China

[2] School of Materials Science and Engineering, Lanzhou Jiaotong University, Lanzhou, PR China

[3] National Green Coating Technology and Equipment Research Center, Lanzhou Jiaotong University, Lanzhou, PR China

[4] CAS Key Laboratory of Bio-based Materials, Qingdao Institute of Bioenergy and Bioprocess Technology, Chinese Academy of Sciences, Qingdao, China

Correspondence
Junfeng Tong and Yangjun Xia, Key Laboratory of Optoelectronic Technology and Intelligent Control of Ministry Education, Lanzhou Jiaotong University, Lanzhou 730070, PR China.
Email: tongjunfeng139@163.com; xiayangjun2015@126.com

Funding information
Natural Science Foundation of Gansu Province, Grant/Award Number: 17JR5RA093; Excellent Team of Scientific Research in Lanzhou Jiaotong University, Grant/Award Numbers: 201705 and 201703; National Natural Science Foundation of China, Grant/Award Numbers: 61404067 and 51463011; Foundation of A Hundred Youth Talents Training, Grant/Award Number: 152022

Compared with benzo[1,2-*b*:3,4-*b*′:5,6-*d*″]trithiophene (BTT), an extended π-conjugation fused ring derivative, dithieno[2,3-*d*:2′,3′-*d*′]benzo[1,2-*b*:3,4-*b*′:5,6-*d*″]trithiophene (DTBTT) has been designed and synthesized successfully. For investigating the effect of extending conjugation, two wide-bandgap (WBG) benzo[1,2-*b*:4,5-*b*′]dithiophene (BDT)-based conjugated polymers (CPs), PBDT-DTBTT, and PBDT-BTT, which were coupled between alkylthienyl-substituted benzo[1,2-*b*:4,5-*b*′]dithiophene bistin (BDT-TSn) and the weaker electron-deficient dibromides $DTBTTBr_2$ and $BTTBr_2$ bearing alkylacyl group, were prepared. The comparison result revealed that the extending of conjugated length and enlarging of conjugated planarity in DTBTT unit endowed the polymer with a wider and stronger absorption, more ordered molecular structure, more planar and larger molecular configuration, and thus higher hole mobility in spite of raised highest occupied molecular orbital (HOMO) energy level. The best photovoltaic devices exhibited that PBDT-DTBTT/PC_{71}BM showed the power conversion efficiency (PCE) of 2.73% with an open-circuit voltage (V_{OC}) of 0.82 V, short-circuit current density (J_{SC}) of 6.29 mA cm^{-2}, and fill factor (*FF*) of 52.45%, whereas control PBDT-BTT/PC_{71}BM exhibited a PCE of 1.98% under the same experimental conditions. The 38% enhanced PCE was mainly benefited from improved absorption, and enhanced hole mobility after the conjugated system was extended from BTT to DTBTT. Therefore, our results demonstrated that extending the π-conjugated system of donor polymer backbone was an effective strategy of tuning optical electronic property and promoting the photovoltaic property in design of WBG donor materials.

KEYWORDS

dithieno[2,3-*d*:2′,3′-*d*′]benzo[1,2-*b*:3,4-*b*′:5,6-*d*″]trithiophene, extending the π-conjugated system, molecular configuration, photovoltaic property

1 | INTRODUCTION

Bulk heterojunction (BHJ) polymer solar cells (PSCs) have attracted extensive focuses from academics and industry because of their unique advantages, such as solution processability, lightweight modules, and low cost for large-area device fabrication.[1,2] To date, the power conversion efficiency (PCE) of BHJ PSCs[3] has reached up to 13%; however, there still falls behind compared with the inorganic solar cells. So further improving the PCE is still vital and highly desired. The photoactive layer of PSCs, fabricated by using a blend of π-conjugated polymers (CPs) and fullerene derivatives, is deemed to be a critical factor determining the PCE of PSCs. Thus, the development of efficient

donor polymers is crucial to further boost up the PCE of PSCs. In general, the high-efficient CPs donor materials should possess following characteristics: (a) widen and strengthen the absorption to match the solar spectrum for acquiring higher short-circuit density (J_{SC}); (b) a lower-lying highest occupied molecular orbital (HOMO) energy level (E_{HOMO}) for maximizing the open-circuit voltage (V_{OC}) and suitable lowest unoccupied molecular orbital (LUMO) energy level (E_{LUMO}) matched with PCBM for obtaining efficient charge separation with low energy loss; (c) ordered microstructure and highly polymer backbone planarity, resulting in higher mobility to facilitate charge transport, which was beneficial for yielding better J_{SC} and fill factor (*FF*); (d) good solubility in organic solvents for solution-processable fabrication process and excellent miscibility with PCBM for forming optimal morphology and nanoscaled phase separation of the interpenetrating network in donor/acceptor blend active layer.[1] Among the numerous donor material, according to their optical bandgaps (E_g^{opt}), polymer donor materials can be classified into low-bandgap (LBG, E_g < 1.6 eV), medium-bandgap (MBG, E_g: 1.6-1.8 eV), and wide-bandgap (WBG, E_g > 1.8 eV) materials.[4] Recently, LBG CPs, such as PNTz4T, PffBT4T-2OD,[2] PCPDTBT,[5] and PTT-DTNT-DT,[6] have attracted growing interesting and achieved higher J_{SC} and charming PCE; however, these CPs usually suffered from the lower V_{OC}. Generally, the LBG polymers were obtained by elevating HOMO and deepening LUMO in order to harvest more sunlight for increasing J_{SC}; unfortunately, the V_{OC} was inevitably impaired because the V_{OC} was directly related to the difference between the E_{HOMO} of donor and the E_{LUMO} of acceptor. So there existed a bottleneck, which was difficult to simultaneously optimize the E_{HOMO} and optical bandgap for achieving efficient PSCs.[1] To overcome this bottleneck, to design and develop the WBG polymers are an effective and facile method, since WBG CPs usually possessed a deepened E_{HOMO} and thus higher V_{OC}; meanwhile, the J_{SC} could be enhanced by expanding absorption spectra when blended with fullerence-free acceptor (ITIC) to form complementary absorption.[7] In contrast to the massive and widely investigated LBG CPs, WBG CPs were ignored to some extent. Therefore, it is urgent and necessary to design and synthesize the highly efficient WBG CPs.

Usually, CPs are composed of rigid CP backbone and peripheral flexible side chain.[8] It has been demonstrated that selecting an appropriate backbone unit to construct high-efficient CPs is of particular importance. Among the numerous subunits, star molecule benzo[1,2-*b*:4,5-*b*′]dithiophene (BDT) has proved to be one the most successful building block because of its high planarity, tunability, and easy synthesis, and thus, plenty of BDT-based high-efficient CPs have been developed.[2,9,10] Inspiring the BDT, another interesting and excellent moiety benzo[1,2-*b*:3,4-*b*′5,6-*d*″]trithiophene (BTT) bearing highly planar and extended aromatic conjugated structure was developed by fusing three thiophene units to a central benzene core by Nielsen in 2011,[11] and thus, many BTT-based CPs have been widely focused and achieved the outstanding photovoltaic performance.[12-17] It has been found that the largely conjugated planarity not only can significantly improve the π overlap of polymer backbone and electron delocalization and thus induce the red-shifted absorption spectra but also can restrict the interannular rotation to reduce the recombination energy of conjugated systems to facilitate photogenerator splite into free charge, which was helpful for facilitating the charge transport.[18-22] In 2013, Hou et al introduced a more extended fused aromatic systematic dithieno[2,3-*d*:2′,3′-*d*′]benzo[1,2-*b*:4,5-*b*′]dithiophene (DTBDT) than bright star BDT into the polymer backbone and synthesized two CPs of PDT-S-T and PBDTTT-S-T. It was found that the backbone of PDT-S-T has a more linear conformation compared with PBDTTT-S-T bearing zigzagged conformation and the intermolecular π-π stacking of the polymer will be enhanced and a more ordered interchain packing could be formed in the film and thus the higher PCE of 7.79% based on PDT-S-T/PC_{71}BM device was achieved, while the PCE of 5.93% for PBDTTT-S-T/PC_{71}BM-based device was observed.[23] Recently, Huo et al also developed a dithienosilolodithiophene (DTTS) unit via enlarging the π-conjugated system of dithieno[3,2-*b*:2′,3′-*d*]silole (DTS) and synthesized LBG CPs of PDTTS and PDTS, respectively, and demonstrated that PDTTS with an enlarged π-conjugated system exhibited a more wider absorption profile, a deeper HOMO energy level, a distinctly better film aggregation, and result in more than one order of magnitude higher mobility. Thus, PDTTS/PC_{71}BM-based device showed simultaneously enhanced V_{OC}, J_{SC}, *FF*, and PCE of 6.33%, which was raised by 97% than PDTS/PC_{71}BM-based device.[24] Apart from tuning the polymer backbone, selecting the side chain was important for enhancing the efficiency of PSCs.[8] As a matter of fact, the flexible side chain has a key role in tuning absorption, photostability, crystallinity, molecular orientation, and the morphology of the active layers.[25,26] As known, the electron donating of alkyloxy is greater than that of alkyl; therefore, P3HOT had a higher E_{HOMO} compared with P3HT and thus got the lower V_{OC}.[27] Following, Hou et al replaced the ester group on thieno[3,4-*b*]thiophene unit with an acyl side chain and prepared the PBDTTT-C, which deepened the E_{HOMO} from −5.01 to −5.12 eV, and thus, the V_{OC} was increased[28] from 0.62 to 0.70 V. Zhang et al demonstrated that more electron-deficient acyl group than alkyl achieved a more broaden absorption band and deepened E_{HOMO}, such variation tended to an improved device performance.[12] On the basis of the above analyses, the design strategy of enlarging the π-conjugated system and selecting the flexible aryl as side chain is effective and desirable for tuning the molecular structure and improving the photovoltaic performance.

Inspired by the aforementioned strategies, herein, we reported a novel large-conjugation dithieno[2,3-*d*:2′,3′-*d*′]benzo[1,2-*b*:3,4-*b*′:5,6-*d*″]trithiophene (DTBTT) building block with an electron-withdrawing alkylacyl group by extending aromitic ring of BTT core, via four-steps chemical synthesis. As shown in Figure 1, one new WBG CP, PBDT-DTBTT composed of alkylacyl-substituted DTBTT and alkylthienyl-substituted BDT units, was designed and prepared. For better comparison, a control polymer PBDT-BTT was synthesized. And the effect of enlarging π-conjugated system on thermal stability, optical, electrochemical property, morphology, and photovoltaic performance of corresponding BHJ active layers was also investigated in detail.

2 | EXPERIMENTAL SECTION

2.1 | Materials

Dichloromethane (DCM) was refluxed over CaH_2 and distilled, and Toluene (Tol) was refluxed and distilled from sodium with

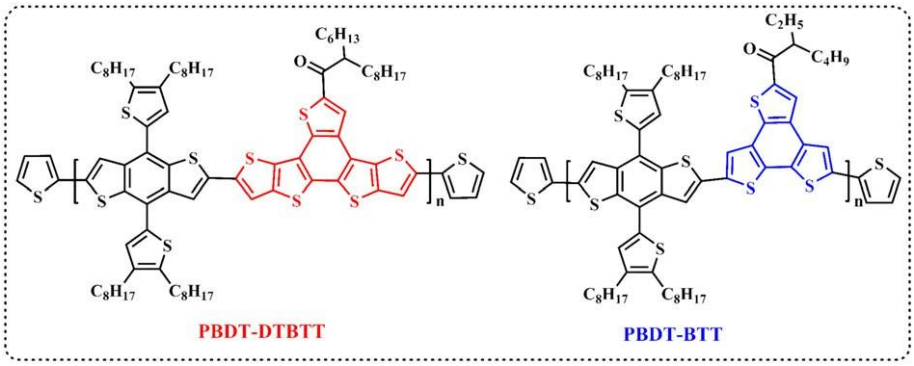

FIGURE 1 Chemical structures of two conjugated polymers PBDT-DTBTT and PBDT-BTT [Colour figure can be viewed at wileyonlinelibrary.com]

benzophenones prior to use. Other commercially available reagents were purchased from Sigma-Aldrich Co, Acros, TCI Chemical Co, and J&K scientific and used without further purification. Bistin comonomer 2,6-bis-(trimethyltin)-4,8-bis(4,5-dioctylthien-2-yl) benzo[1,2-*b*:4,5-*b*′]dithiophene (BDT-TSn),[29] 5-(2-ethylhexanoyl) benzo[1,2-*b*:3,4-*b*′:5,6-*d*″]trithiophene,[11] alcohol-solubled conjugated copolymer poly[(9,9-bis(3′-(*n*,*n*-dimethylamino)propyl)-2,7-fluorene)-*alt*-2,7-(9,9-dioc-tylfluorene)] (PFN),[30] and 3,9-bis-(2-methylene-(3-(1,1-dicyanomethylene)-indanone))-5,5,11,11-tetrakis-(4-hexylphenyl) dithieno[2,3-*d*:2′,3′-*d*′]-*s*-indaceno[1,2-*b*:5,6-*b*′]dithiophene (ITIC)[7] were synthesized according to the previously reported procedure and characterized by ^{1}H nuclear magnetic resonance (NMR) before use.

2.2 | General method

^{1}H NMR and ^{13}C NMR spectra were measured with Bruker DRX 400 or DRX 500 spectrometer (Rheinstetten, Germany) operating at 400 and 500 MHz; tetramethylsilane (TMS) and deuterated chloroform were used as the internal reference and deuterated reagent, respectively. The number-average molecular weight (M_n) and the weight-average molecular weight (M_w) were measured on gel permeation chromatography (GPC), THF was invoked as the mobile phase, and linear polystyrene was used as the standard. The thermal stability of the material was determined by a TGA 2050 thermal analysis system under the protection of N_2 (flow rate 20 mL min^{-1}) at a heating rate of 10°C min^{-1} and range of 25°C to 600°C. Ultraviolet-visible (UV-vis) absorption spectrum was conducted on a UV 1800 ultraviolet ray absorption spectrometer. The redox potential of the material was identified by using cyclic voltammetry (CV). It was measured on a CHI600D electrochemical work station with a standard three-electrode system. The auxiliary electrode is a platinum wire, the working electrode is a platinum-carbon electrode, and the reference electrode is Ag/$AgNO_3$; meanwhile, tetrabutylammonium hexafluorophosphate (Bu_4NPF_6) was prepared into a 0.1 mol L^{-1} acetonitrile (CH_3CN) solution as an electrolyte. The surface roughness and morphology of the thin films were monitored by atomic force microscopy (AFM) on an MFP-3D-SA system in tapping mode. The X-ray diffraction (XRD) pattern was measured on a PANalytical X'Pert PRO instrument with Cu-Kα as the emission source. The interfacial distance (*d*) can be obtained by Bragg's law ($\lambda = 2d\sin\theta$, where the artificial ray wavelength [λ] was 1.54 Å, *d* was the mirror distance, and ϑ was the diffraction angle).

2.3 | Preparation and characterization of PSC devices

The indium tin oxide (ITO) patterned glass that sheet resistance is 10 to 15 Ω/square was cleaned with ultrasonic treatment in detergent and deionized water, followed by acetone and isopropanol (iPrOH) sequentially. After oxygen plasma cleaning for 5 minutes, a thin layer of PFN (~5 nm) was spin casted onto the precleaned ITO glass at 2500 rpm. The polymer donor and acceptor of $PC_{61}BM$ or $PC_{71}BM$ were dissolved in chlorobenzene (CB) in different weight ratios, and the total concetration of the donar/acceptor blending solution was 8 mg/mL. The device was transferred to a glove box, where deposited on the top of the PFN-modified ITO by spin casting as the active layers with a thickness ranging in the 100 to 110 nm. Subsequently, a 10 nm MoO_3 and 100 nm silver layer were successively evaporated on the top of the active layer with a shadow mask under vacuum of (1-5) × 10^{-5} Pa. The same procedures were applied to the devices with ITIC as electron acceptor materials expect that the PCBM was replaced by ITIC. The overlapping area between the cathode and anode defined a pixel size of device of 0.1 cm^2. The thickness of the active layer was determined by varying the spin-coating speed and measured on a profile system (BRUKER VDS-9400 QS). The thickness of the evaporated cathode was monitored by a quartz crystal thickness/ratio monitor (SI-TM206, Shenyang Science). Photovoltaic performance of devices was tested under one sun, AM 1.5 G (air mass 1.5 global) condition using an AAA class solar simulator (XES-70S1, San-EI Electric) with irradiation of 100 mW cm^{-2}. The current density-voltage (*J*-*V*) characteristics were measured by a computer-controlled Keithley 2400 source measurement unit. The external quantum efficiency (EQE) was performed by using a 7-SCSpecIII acquisition system (Bejing 7-Star Opt).

2.4 | Synthesis of comonomers

2.4.1 | Synthesis of 2,8-dibromo-5-(2-ethylhexanoyl) benzo[1,2-b:3,4-b′:5,6-d″]trithiophene (BTTBr$_2$)[11]

A solution of 5-(2-ethylhexanoyl)benzo[1,2-*b*:3,4-*b*″:5,6-*d*‴] trithiophene (1.21 g, 3.20 mmol) and *N*-bromosuccinimide (NBS, 1.30 g, 7.36 mmol) in anhydrous *N*,*N*-dimethyl-formamide (DMF, 100 mL) was stirred at 50°C in the dark over night, after which the reaction mixture was quenched with water, extracted with chloroform, washed with water, and finally dried over anhydrous sodium sulfate (Na_2SO_4) and concentrated to afford the crude product. Purification by column chromatography (silica, petroleum ether) and subsequently recrystallized from methanol (MeOH) finally afforded the title compound (1.05 g, 61%) as a yellow solid. ^{1}H NMR (400 MHz, $CDCl_3$): δ 8.20 (s, 1H), 7.68 (s, 1H), 7.58 (s, 1H), 3.35 to 3.19 (m, 1H), 1.93 to 1.83 (m, 2H), 1.70 to 1.58 (m, 2H), 1.36 to 1.26 (m, 4H), 0.96 (t, *J* = 7.4 Hz, 3H), 0.87 (t, *J* = 6.8 Hz, 3H). ^{13}C NMR (400 MHz, $CDCl_3$): δ 198.57, 144.43, 135.20, 133.11, 131.53, 131.38, 130.99, 126.30, 125.54, 125.21, 114.51, 114.37, 50.08, 32.31, 29.96, 29.71, 25.99, 22.79, 14.05, 12.12. Anal. Calcd for $C_{20}H_{18}Br_2OS_3$: C, 45.29%; H, 3.42%. Found, C, 45.71%; H, 3.12%.

2.4.2 | Synthesis of 2,3-dibromo-5-(2-hexyldecanoyl) thiophene (2)

Aluminium chloride (16.55 g, 124.0 mmol) was slowly added into an ice-cooled solution of 2,3-dibromothiophene (15.00 g, 62.00 mmol) and 2-hexyldecanoyl chloride (22.76 g, 83.10 mmol) in DCM (60 mL). The reaction mixture was stirred for 2 hours, and the mixture was warmed up to room temperature. Next, the mixture was poured into 100 mL water and extracted with ethyl macetate (10 mL × 3), and the organic layers were washed with water two times. After dried over anhydrous Na_2SO_4, the filtrate was concentrated in vaccuo. The residue was purifiedon a silica gel column, eluting with petroleum ether and DCM to afford (2) as an oily yellow solid (19.30 g, 65%). ^{1}H NMR (400 MHz, $CDCl_3$): δ 7.50 (s, 1H), 3.35 to 3.19 (m, 1H), 1.98 to 1.90 (m, 2H), 1.70 to 1.63 (m, 2H), 1.43 to 1.24 (m, 20H), 0.88 (t, *J* = 7.6 Hz, 3H), 0.84 (t, *J* = 6.8 Hz, 3H). Anal. Calcd for $C_{20}H_{32}Br_2OS$: C, 50.01%; H, 6.71%. Found, C, 50.12%; H, 6.92%.

2.4.3 | Synthesis of 2-(2-hexyldecanoyl)-4,5-bis(thieno[3,2-b]thiophen-3-yl)thiophene (3)

A suspension of 2 (11.05 g, 23.12 mmol), 4,4,5,5-tetramethyl-2-(thieno[3,2-*b*]-thiophen-3-yl)-1,3,2-dioxaborolane (17.22 g, 64.74 mmol), and potassium carbonate (41.48 g, 0.30 mol) in Tol (100 mL) and ethanol (40 mL) was degassed by bubbling with argon atmosphere for 2 hours. Then, Pd (PPh_3)$_4$ (0.40 g, 0.346 mmol) was added, and the reaction mixture was heated at 110°C for 20 hours. The reaction mixture was quenched with water and extracted with ethyl macetate (10 mL × 3), and the organic layers were washed with water two times. After dried over anhydrous Na_2SO_4 and concentrated to afford the crude product, which was purifiedon a silica gel column, eluting with petroleum ether and DCM and subsequently recrystallized from Tol/MeOH, finally afforded the title compound (7.47 g, 54%) as a pale yellow solid. ^{1}H NMR (500 MHz, $CDCl_3$): δ 8.40 (s, 1H), δ 7.98 (s, 1H), δ 7.94 (s, 1H), 7.68 (d, *J* = 5.1 Hz, 1H), 7.62 (d, *J* = 5.1 Hz, 1H) 7.46 (d, *J* = 5.0 Hz, 1H), 7.43 (d, *J* = 5.0 Hz, 1H), 3.35 to 3.19 (m, 1H), 1.96 to 1.90 (m, 2H), 1.70 to 1.63 (m, 2H), 1.43 to 1.24 (m, 20H), 0.86 to 0.80 (m, 6H). Anal. Calcd for $C_{32}H_{38}OS_5$: C, 64.17%; H, 6.39%. Found, C, 64.95%; H, 6.30%.

2.4.4 | Synthesis of 10-(2-hexyldecanoyl) dithieno[2,3-d:2′,3′-d′]benzo[1,2-b:3,4-b′: 5,6-d″] trithiophene

Boron trifluoride diethyl etherate (BF_3OEt_2, 1.15 g, 8.13 mmol) was added into an ice-cooled solution of 3 (3.74 g, 6.25 mmol) in anhydrous DCM (290 mL) after which 2,3-dichloro-5,6-dicyano-1,4-benzoquinone (DDQ, 1.70 g, 7.5 mmol) was added portion wise during 10 minutes. The reaction mixture was warmed up to room temperature for overnight and was subsequently quenched by addition of zinc (4.12 g, 63.4 mmol) and MeOH (120 mL). After stirring over night, the mixture was filtered off, and the filtrates were washed with water and dried over anhydrous Na_2SO_4. After concentrated, the crude product was purified on a silica gel column, eluting with petroleum ether and DCM, and recrystallisation (MeOH) afforded the title compound (1.75 g, 47%) as a yellow solid. ^{1}H NMR (500 MHz, $CDCl_3$): δ 8.48 (s, 1H), 7.68 (d, *J* = 5.1 Hz, 1H), 7.61 (d, *J* = 5.1 Hz, 1H), 7.46 (d, *J* = 5.0 Hz, 1H), 7.43 (d, *J* = 5.0 Hz, 1H), 3.35 to 3.19 (m, 1H), 1.94 to 1.90 (m, 2H), 1.70 to 1.63 (m, 2H), 1.43 to 1.24 (m, 20H), 0.86 to 0.80 (m, 6H). Anal. Calcd for $C_{32}H_{36}OS_5$: C, 64.38%; H, 6.08%. Found, C, 65.21%; H, 6.45%.

2.4.5 | Synthesis of 2,7-dibromo-10-(2-hexyldecanoyl)dithieno[2,3-d:2′,3′-d′]benzo[1,2-b: 3,4-b′:5,6-d″]trithiophene (DTBTTBr$_2$)

A solution of 4 (1.75 g, 2.93 mmol) and NBS (1.19 g,7.36 mmol) were dissolved in anhydrous DMF (100 mL) and then stirred at 50°C in the dark over night, after which the solution was poured into water, extracted with chloroform, washed with water, and finally dried over anhydrous sodium sulfate and concentrated to afford the crude product. Purification by column chromatography (silica, petroleum ether) and subsequent recrystallisation (MeOH) afforded the title compound (1.32 g, 60%) as a yellow solid. ^{1}H NMR (400 MHz, $CDCl_3$): δ 8.15 (s, 1H), 7.37 (s, 1H), 3.51 to 3.43 (m, 1H), 1.98 to 1.90 (m, 2H), 1.70 to 1.63 (m, 2H), 1.43 to 1.24 (m, 20H), 0.88 (t, *J* = 7.6 Hz, 3H), 0.84 (t, *J* = 6.8 Hz, 3H). ^{13}C NMR (400 MHz, $CDCl_3$): 198.25, 144.72, 135.81, 135.33, 134.87, 133.97, 133.81, 133.392, 132.90, 129.79, 125.51, 125.02, 123.31, 122.72, 116.07, 115.06, 48.78, 33.18, 33.12, 31.88, 31.79, 29.97, 29.64, 29.55, 29.37, 29.19, 27.98, 27.96, 22.71, 22.68, 14.13, 14.11. Anal. Calcd for $C_{32}H_{34}Br_2OS_5$: C, 50.92%; H, 4.54%. Found, C, 60.11%; H, 5.04%.

2.5 | Synthesis of polymer PBDT-BTT

In a 25 mL three-neck flask, a solution of BTTBr$_2$ (79.5 mg, 0.15 mmol) and BDT-TSn (169.4 mg, 0.15 mmol) were dissolved in

a mixture of Tol (7 mL) and DMF (0.6 mL). The solution was purged with argon for 45 minutes, and then, $Pd_2(dba)_3$ (1.5 mg) and P(*o*-tol)$_3$ (3 mg) were added into the solution. The reaction mixture was stirred at 105°C and refluxed for 36 hours under argon atmosphere and then cooled down to room temperature. The mixture was precipitated in a vigorously stirred MeOH (200 mL). The crimson solid was recovered by filtration, and the crude polymer was extracted with ethanol, acetone, hexane, and Tol in a Soxhlet apparatus, successively. The solution of the polymer was condensed to 20 mL and then poured into MeOH (200 mL). The precipitation was collected and completely dried in vacuo to afford target polymer. (Yield: 75%). M_n = 43.7 kDa, PDI = M_w/M_n = 1.69. Anal. Calcd for $C_{78}H_{96}O_2S_9$: C, 72.01%; H, 7.23%. Found, C, 72.31%; H, 7.45%.

2.6 | Synthesis of polymer PBDT-DTBTT

The synthesis procedure of PBDT-DTBTT was identical to that of PBDT-BTT except that the bistin compound BDT-TSn (169.4 mg, 0.15 mmol) and the dibromo compound $DTBTTBr_2$ (113.2 mg, 0.15 mmol) were used in place of the previous monomer. Yield (85%). M_n = 50.6 kDa with PDI of 1.77. Anal. Calcd for $C_{90}H_{112}OS_{11}$: C, 69.18%; H, 7.22%. Found, C, 71.61%; H, 7.47%.

3 | RESULTS AND DISCUSSION

3.1 | Synthesis and characterization

The comonomer $BTTBr_2$ was synthesized according to previous literature.[11] Synthesis routes of comonomer $DTBTTBr_2$ and copolymers PBDT-BTT and PBDT-DTBTT were carried out according to Scheme 1. DTBTT was prepared via following four steps: (a) starting from 2,3-dibromothiophene 1, a solubilising side chain was incorporated by the Friedel-Crafts acylation to yield intermediate 2; (b) 2 was reacted with 4,4,5,5-tetramethyl-2-(thieno[3,2-*b*]thiophen-3-yl)-1,3,2-dioxaborolane via the Suzuki-Miyaura cross-coupling reaction to give intermediate 3; (c) following 3 was oxidatively ring-closed assisted by DDQ to form the DTBTT; and (d) the dibromide $DTBTTBr_2$ was brominated with NBS in DMF at 50°C. The structure of intermediates and comonomers was confirmed by ^{1}H NMR and ^{13}C NMR (Figures S1-S4).

The studied copolymers PBDT-BTT and PBDT-DTBTT were synthesized between dibromides $BTTBr_2$ or $DTBTTBr_2$ and bistin BDT-TSn via the palladium-catalyzed Stille cross-coupling reaction.[31] The copolymers were end capped with 2-tributylstannyl-thiophene and 2-bromothiophene to remove bromo and trimethylstannyl end groups.[32] After the polymerization, the reaction mixture was poured into MeOH, and the precipitated copolymers were collected and

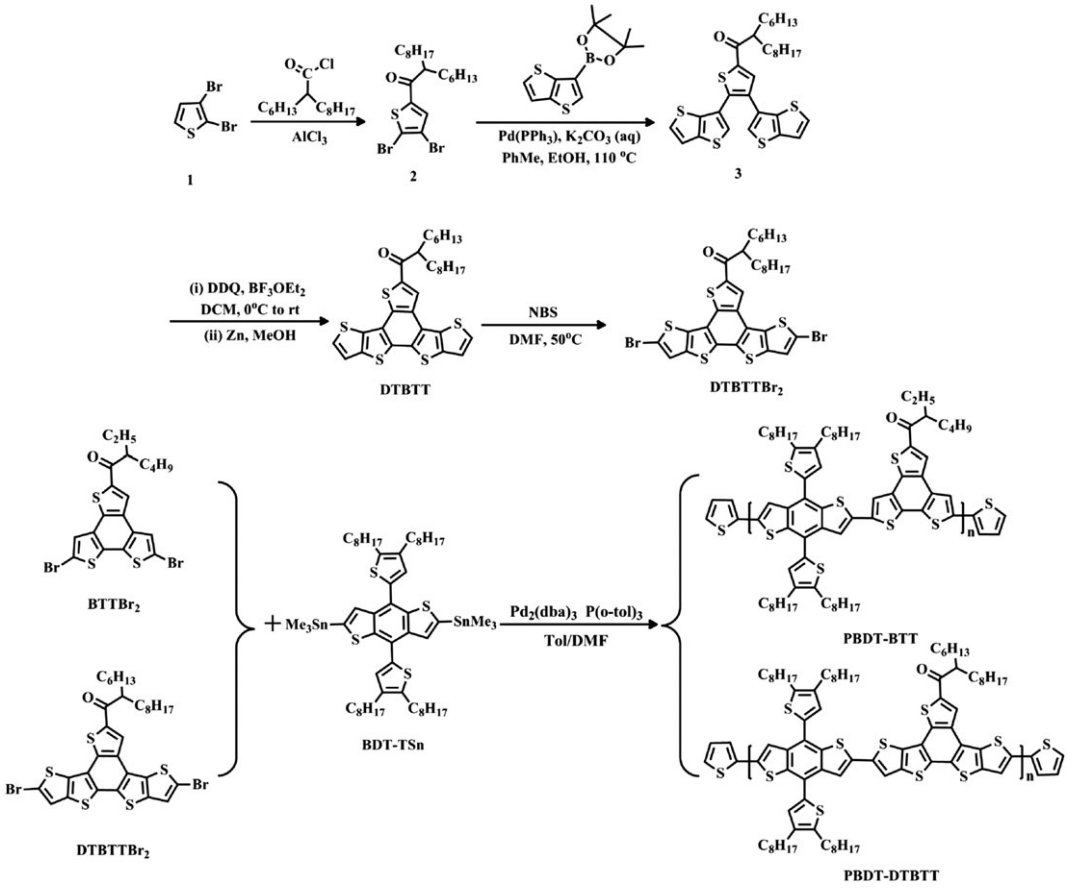

SCHEME 1 Synthetic routes of dibromide monomer $DTBTTBr_2$ and polymer PBDT-BTT and PBDT-DTBTT

extracted with ethanol, acetone, hexane, and Tol solvent in a Soxhlet extractor to remove the residue catalyst and oligomers. Then, the concentrated solutions of the copolymers in Tol were poured into MeOH again, and the precipitated copolymers were collected with the yields of 75% to 85%. The polymers PBDT-BTT and PBDT-DTBTT can be easily dissolved in common organic solvents, such as THF, Tol, chloroform, chlorobenzene (CB), and *o*-dichlorobenzene (*o*-DCB). The number-average molecular weight (M_n) of the PBDT-BTT and PBDT-DTBTT determined by GPC in THF with polystyrene standards was about 43.7 kDa with PDI of 1.69 and 50.6 kDa with PDI of 1.77, respectively (Table S1). Thermogravimetric analysis (TGA) measurements were carried out to evaluate the thermal stability of the two polymers, and the TGA plots found that the decomposition temperatures (T_d, 5% weight-loss temperature) are 419°C and 425°C for PBDT-BTT and PBDT-DTBTT, respectively (see Figure S5 and Table S1), and indicated that two copolymers exhibit good thermal stability. Meanwhile, the results revealed that PBDT-DTBTT possesses the more higher stability than that of PBDT-BTT, which may be originated from the enlarged conjugated planarity.

3.2 | Optical properties

The absorption properties of the copolymers were characterized through UV-1800 spectrophotometer. The UV-vis absorption spectra of PBDT-DTBTT and PBDT-BTT in dilute CB solution and solid thin film were presented in Figures 2 and S6A, respectively; the corresponding data were listed in Table 1. Both copolymers indicated the similar absorption profiles, that is, one weak absorption in high energy region, which was attributed π-π* transition of polymer backbone; one strong absorption placed in low energy region was assigned to the intramolecular charge transfer between BDT and alkylacyl-substituted BTT/DTBTT units,[12,15] as well as an obvious shoulder peak, which was related to aggregation.[33,34] On going from solution to film, the red-shifted values of the maximal absorption peak (λ_{max}^{abs}) and absorption band-edge (λ_{onset}^{abs}) transition were 1 and 0 nm for PBDT-BTT and 2 and 5 nm for PBDT-DTBTT, respectively. These results indicated that the PBDT-DTBTT with an extended π-conjugated system possessed a more stronger intermolecular interaction, which was confirmed by the latter XRD analysis and density functional theory (DFT) calculation. Similarly, the extended conjugated structure also resulted in a slightly small optical bandgaps (E_g^{opt}) calculated from the absorption edges of solid films of 2.04 eV for PBDT-DTBTT, while 2.07 eV for PBDT-BTT. Aparting from the absorption range, the absorption coefficient was also an important parameter for judging the harvesting solar light of polymer materials.[6,22] Thus, the molar absorption coefficients (ε) of two polymers were measured as shown in Figure S7. And the ε values were found to be 66 808 and 146 778 L mol^{-1} cm^{-1} for PBDT-BTT and PBDT-DTBTT, respectively, indicating a 2.2 times increased molar absorption coefficients when the conjugated plane was increased from BTT to DTBTT.

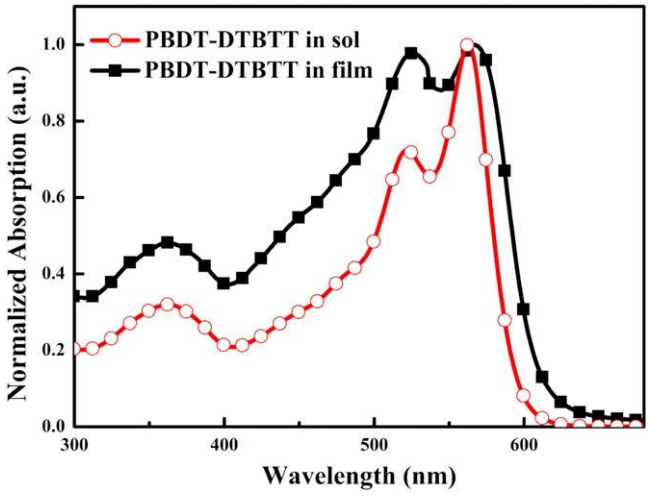

FIGURE 2 Absorption spectra of PBDT-DTBTT in the diluted CB solution and solid thin film [Colour figure can be viewed at wileyonlinelibrary.com]

In order to investigate the molecular intrinsic properties of the copolymers, their temperature-dependent absorption spectra (TD-Abs) in CB solution were further monitored (Figures 3 and S6B). When the temperature was increased from 25°C to 105°C, for PBDT-BTT, red-shifted value of 10 nm (from 511 to 521 nm) of 0 to 1 peak was observed, as well as the 0 to 0 peak gradually declined and disappeared completely until 85°C. Meanwhile, on the heating process, the absorption profile for 0 to 1 and 0 to 0 peaks of PBDT-DTBTT remained unchanged, and the tiny blue-shift values of approximately 2 nm (from 562 to 560 nm for 0-0 peak and from 525 to 523 nm for 0-1 peak) were seen, which may be because of the fact that the effective conjugation length would be decreased because of increased torsion angle of adjacent elements or decreased coplanarity of the building blocks in the repeating units during heating process; thus, led to the absorption spectrum is blue shifted. Meanwhile, the shoulder peaks associated with the intermolecular π-π* transitions are significantly weakened when the temperature elevated.[6,29] So we can infer that PBDT-DTBTT with an extended conjugated system exhibited a more pronounced aggregation than that of PBDT-BTT.

TABLE 1 Optical and electrochemical characteristics of PBDT-BTT 和 PBDT-DTBTT

Polymer	Solution λ_{max} (nm)	λ_{sh} (nm)	Film λ_{max} (nm)	λ_{sh} (nm)	λ_{onset} (nm)	E_g^{opta} (eV)	φ_{ox}^{onset} (V)	E_{HOMO}^{b} (eV)	E_{LUMO}^{c} (eV)
PBDT-BTT	356, 511	551	351, 512	551	598	2.07	0.74	−5.43	−3.36
PBDT-DTBTT	364, 522	562	363, 524	567	609	2.04	0.65	−5.35	−3.31

[a]Calculated from the onset wavelength of the film absorption spectra ($E_g^{opt} = 1240/\lambda_{onset}^{film}$).

[b]Calculated according to the equation ($E_{HOMO} = -e\,\varphi_{ox}^{onset} + 4.69$] (eV).

[c]Calculated according to the equation $E_{LUMO} = E_{HOMO} + E_g^{opt}$ (eV).

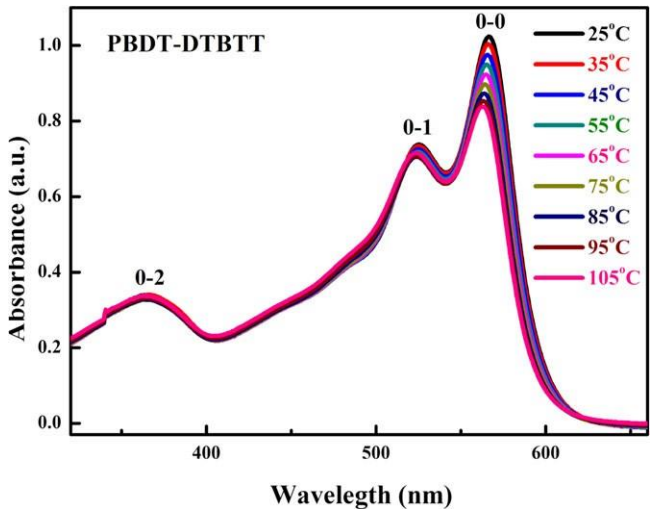

FIGURE 3 TD-Abs spectra for PBDT-DTBTT in diluted CB solution (temperature ranged from 25°C to 105°C with a 10°C interval) [Colour figure can be viewed at wileyonlinelibrary.com]

3.3 | XRD analysis

To further explore the influence of extending the π-conjugated system of polymer backbone on the molecular arrangement and crystallization properties of the polymer film, XRD diffraction was carried out to analyze the aggregation behavior of PBDT-BTT and PBDT-DTBTT in solid film. The polymer thin films were cast from CB solution onto a glass substrate, and the solvent was naturally volatilized to form a uniform polymer film. As shown in Figures 4 and S8, the π-π stacking peaks of PBDT-BTT and PBDT-DTBTT were located at 2θ = 23.5 and 2θ = 24.1, respectively, corresponding to the *d* spacings of 3.91 and 3.75 Å based on Bragg's law (ie, $\lambda = 2d\sin\theta$).[35] Meanwhile, in a small-angle region, only PBDT-DTBTT provided the peak at 2θ = 3.95°, corresponding to interlayer *d* spacing of 22.29 Å. Obviously, the comparison of XRD patterns suggested that PBDT-DTBTT with extended π-conjugated system showed a more ordered interchain structure and higher crystallinity than that of PBDT-BTT. This was in accordance with the preliminary conclusions drawn from UV-vis absorption spectra.

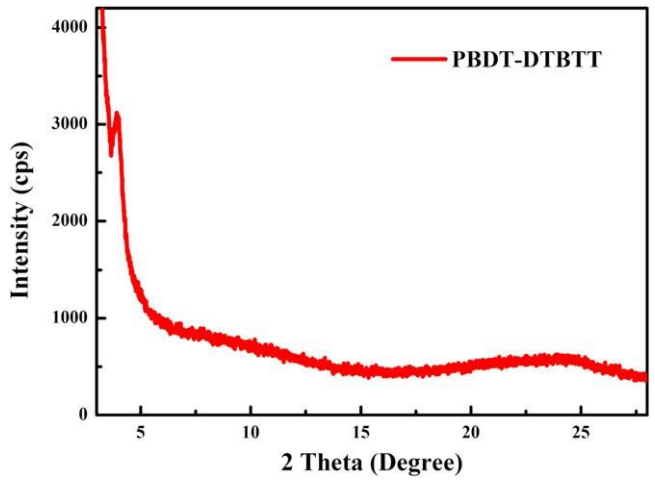

FIGURE 4 X-ray diffraction (XRD) patterns of the pristine PBDT-DTBTT films casted from CB onto a glass substrate [Colour figure can be viewed at wileyonlinelibrary.com]

3.4 | Electrochemical properties

The E_{HOMO} and E_{LUMO} are very important for selecting matched donor and acceptor materials in PSCs. The HOMO/LUMO energy levels of PBDT-BTT and PBDT-DTBTT were measured by carrying out CV, the $Ag/AgNO_3$ electrode and glass carbon as the reference and working electrode, respectively, as shown in Figures 5A and S9. The onset oxidation potentials of PBDT-BTT and PBDT-DTBTT were 0.74 and 0.66 V, respectively. And the $Ag/AgNO_3$ reference electrode was internally calibrated by the ferrocene-ferrocenium (Fc/Fc^+) system to be −4.69 eV in this work. Therefore, the HOMO energy levels can be calculated according to the equation, $E_{HOMO} = -e(\varphi_{ox}^{onset} + 4.69)$ (eV),[36] and were approximately −5.43 eV for PBDT-BTT and −5.35 eV for PBDT-DTBTT, respectively (Table 1). The trend of E_{HOMO} was similar with the other CPs system when the conjugated system was extended.[24,37] The LUMO levels of the polymers were obtained from the HOMO levels and corresponding optical bandgaps. Thus, the calculated LUMO energy levels for the polymers were −3.36 and − 3.31 eV, respectively.[38] For more intuitive comparisons, the energy-level diagram of the polymer donors and acceptors (ITIC and $PC_{71}BM$) was shown in Figure 5B. It can be found that the energy levels of both two copolymers were larger than the energy levels of ITIC and $PC_{71}BM$ by more than 0.3 eV. It is possible to provide sufficient driving force to perform efficient exciton dissociation at the donor and acceptor interfaces. So it could be inferred that both $PC_{71}BM$ and ITIC were suitable for using as effective acceptors to

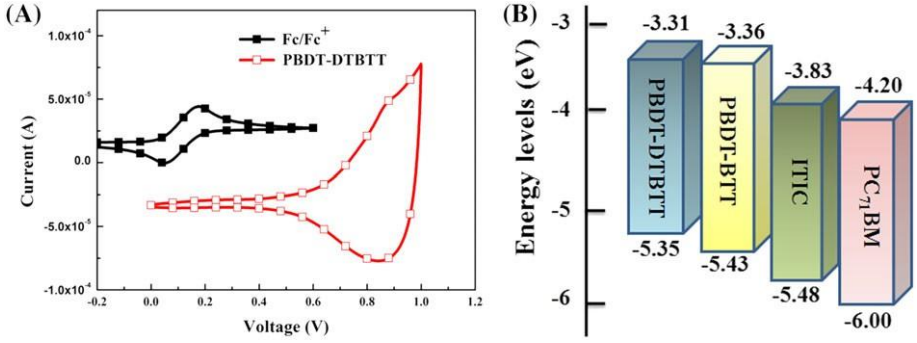

FIGURE 5 (A) Cyclic voltammetry curve of the PBDT-DTBTT film and (B) electrochemical energy level diagram of polymer donors (PBDT-DTBTT and PBDT-BTT) and acceptors (ITIC and $PC_{71}BM$) [Colour figure can be viewed at wileyonlinelibrary.com]

match well with the polymer donors with regard to electronic energy level.[1]

3.5 | Theoretical calculations

To better investigate the effect of increasing the conjugated length and conjugated planarity on the electronic properties of these polymers, the DFT analysis of the polymers' model compound was carried out at the B3LYP/6-31G* basis set by using the Gaussian 09 program suite.[39] For simplifying the calculation process, the trimer compounds of the polymer were selected for simulation. The carbonyl side chains on BTT and DTBTT were both simplified into ethanoyl and the octyl side chain of BDT replaced by methyl. It was obviously seen from Figure 6 that the HOMO wave function was delocalized along the polymer backbone, while two polymers had a good delocalized LUMO wave function. Furthermore, the calculated E_{HOMO}, E_{LUMO}, and E_g were about −4.96, −2.48, and 2.48 eV for PBDT-BTT and −4.91, −2.50, and 2.41 eV for PBDT-DTBTT, respectively, which were consistent with the results obtained from the CV measurements. Additionally, we could see that PBDT-DTBTT showed the more linear conformation than that of PBDT-BTT, since the linear molecular structure was prone to yield the better charge mobility and thus efficient photovoltaic devices.[6,23]

3.6 | Photovoltaic properties

To further explore the photovoltaic properties of these two copolymers, solar cell devices with the architecture of ITO/PFN/donor:acceptor (D/A)/MoO_3/Ag were prepared.[40] Where PBDT-BTT and PBDT-DTBTT were used as electron donor in PSCs, the widely used fullerene derivatives $PC_{61}BM$ or $PC_{71}BM$ were chosen as electron acceptor. Under AM 1.5 G illumination at 100 mW cm^{-2} using solar simulator, the current density-voltage (*J-V*) characteristics were measured and shown in Figure S10, and their detailed photovoltaic parameters were listed in Table S2. The D/A weight ratio of these two polymers: $PC_{61}BM$ was firstly both optimized from 1:1, 1:1.5, to 1:2. We found that the devices with D/A weight ratio of 1:1.5 for PBDT-DTBTT and 1:2 for PBDT-BTT showed the optimal photovoltaic performance. For PBDT-DTBTT, at low feed ratio of (D/A = 1:1), the cell showed a V_{OC} of 0.74 V, a J_{SC} of 3.91 mA cm^{-2}, and an *FF* of 61.37%, resulting in a PCE of 1.76%. When the D/A ratio was changed to 1:1.5, the V_{OC} and J_{SC} were increased up to 0.85 V and 5.98 mA cm^{-2}, respectively, regardless of declined *FF*, and thus, an increased PCE of 2.62% was achieved. Moreover, with the D/A ratio was further increased to 1:2, the V_{OC} and J_{SC} both decreased in spite of a slightly raised *FF*, leading to a decreased PCE. As for PBDT-BTT, the optimal D/A ratio was determined to be 1:2, and corresponding maximum PCE of 1.98 was achieved, with V_{OC} = 0.85 V, J_{SC} = 5.05 mA cm^{-2}, and *FF* = 46.03%. As shown in Figure S10, these EQE curves confirmed the variations of J_{SC} in *J-V* measurement, and the increase of EQE response ranging from 300 to 420 nm corresponded to the contribution of $PC_{61}BM$ when the D/A ratio was elevated.

Since $PC_{71}BM$ has the similar electronic properties to $PC_{61}BM$ hut, a considerably higher absorption coefficient, and broader absorption spectrum,[41] thus, $PC_{71}BM$ replaces $PC_{61}BM$ as the electron acceptor to further optimize the photovoltaic property. The weight ratio of PBDT-DTBTT:$PC_{71}BM$ was fixed at 1:1.5, while one of PBDT-BTT:$PC_{71}BM$ was about 1:2. As shown in Figure 7 and Table S2, the PBDT-DTBTT-based device showed a slight increase in J_{SC} (from 5.98 to 6.29 mA cm^{-2}) and *FF* (from 51.31% to 52.45%) but a declined V_{OC} (from 0.85 to 0.82 V), therefore resulted in an slightly increased PCE of 2.73%. Under similar optimization, PBDT-BTT-based device exhibited an unchanged PCE of 1.98%. Obviously, these

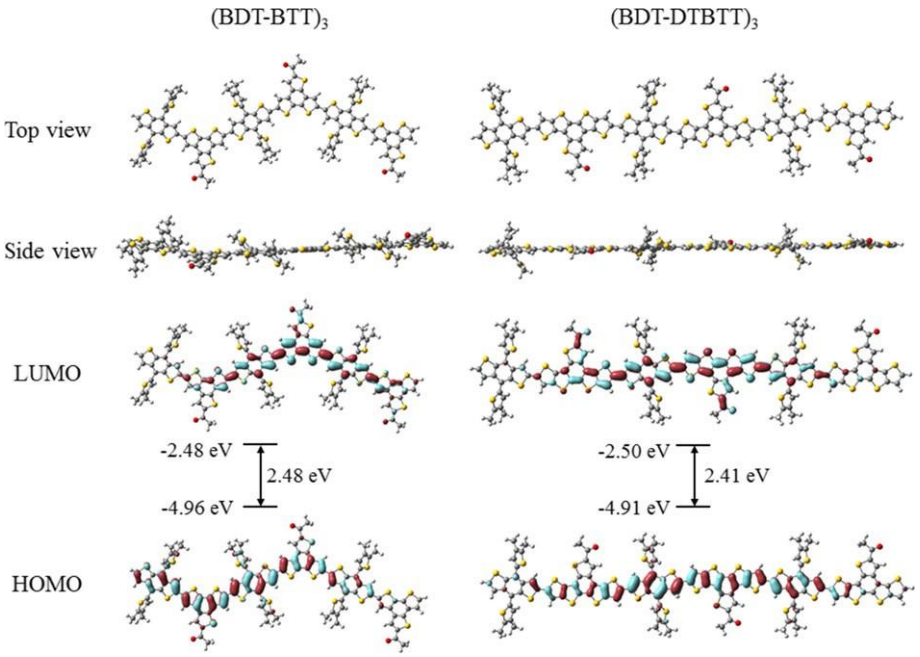

FIGURE 6 Molecular backbone geometries and frontier molecular orbital surfaces of highest occupied molecular orbital (HOMO) and lowest unoccupied molecular orbital (LUMO) by density functional theory (DFT) of compounds PBDT-BTT and PBDT-DTBTT with the B3LYP/6-31G basis set [Colour figure can be viewed at wileyonlinelibrary.com]

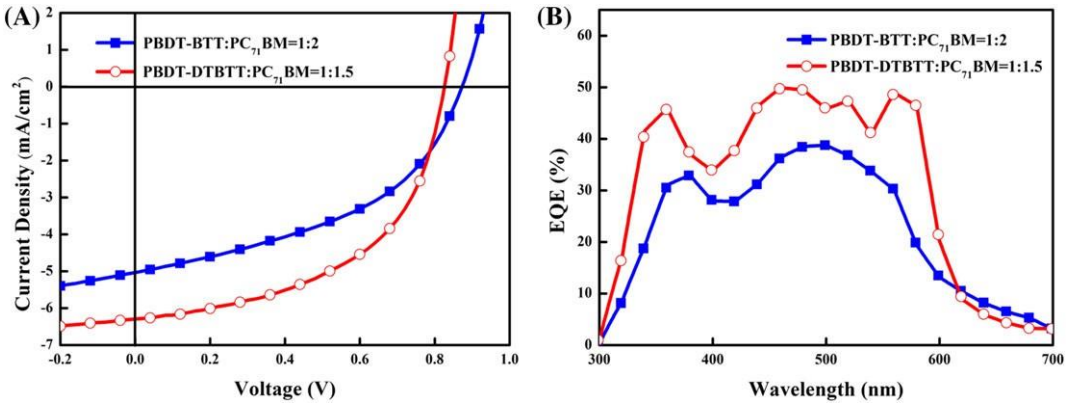

FIGURE 7 The (A) *J-V* curves and (B) EQE spectra of the optimized polymer solar cells (PSCs) based on polymers PBDT-BTT and PBDT-DTBTT with different weight ratio to $PC_{71}BM$ [Colour figure can be viewed at wileyonlinelibrary.com]

variations agreed well with corresponding EQE curves in Figure S10. It was noted that PBDT-DTBTT:$PC_{71}BM$-based device showed a distinct EQE enhancement ranged from 440 to 500 nm, which can account for an increase in J_{SC}.

On the other hand, in view of complementary absorption and suitable molecular energy levels with respect to nonfullerene PSCs, we also fabricated fullerene-free PSCs by employing PBDT-DTBTT and PBDT-BTT as electron donor materials, and a notable nonfullerene-based small molecule named as ITIC was used as electron acceptor material. The *J-V* curves and corresponding photovoltaic date were listed in Figure S12 and Table S3, respectively. The optimal photovoltaic parameters based on PBDT-DTBTT/ITIC and PBDT-BTT/ITIC were given in Figure 8 and Table 2, respectively. The PCEs of the blend films of PBDT-DTBTT and PBDT-BTT displayed poor PCE of 1.33% and 1.76%, with higher V_{OC} of 0.95 and 0.97 V but moderate J_{SC} of 4.09 and 5.55 mA cm^{-2} and miserable *FF* of 34.22% and 34.63%. As expected, these devices used ITIC as electron acceptor exhibited a greatly enhanced V_{OC} compared with polymer: PCBM system, which was benefited from the raised E_{LUMO} of ITIC as the V_{OC} was related to the difference of E_{HOMO} of donor polymer and E_{LUMO} of acceptor material.[1] Unfortunately, although the absorption and EQE response of ITIC-based devices were greatly extended to 800 nm (Figures S11B and S12), they never exhibited the desired higher J_{SC}. And the lower EQE values of approximately 25% were observed, which were also in accord with the J_{SC} values from the corresponding *J-V* measurement.

Going through a series of optimization processes, such as D/A ratio, $PC_{71}BM$ instead of $PC_{61}BM$, ITIC as electron donor, the best *J-V* curve and the related optimal photovoltaic parameters were also given in Figure 7 and Table 2, respectively. The PBDT-DTBTT/PC_{71}BM-based cell displayed optimal PCE of 2.73, a V_{OC} of 0.82 V, a J_{SC} of 6.29 mA cm^{-2}, and *FF* of 52.45%, while PBDT-BTT-based cell exhibited the best PCE of 1.98%, with slightly elevated V_{OC} of 0.87 V, J_{SC} of 5.03 mA cm^{-2}, and *FF* of 45.20%. The decreased trend of V_{OC} was consistent with the E_{HOMO} variations both in CV measurement and DFT prediction after the extended conjugated system from BTT to DTBTT. The increased J_{SC} and *FF* could be partially explained the wider and stronger absorption, enhanced space-charge limited current (SCLC) hole mobility, which will be discussed in the following section. As can be seen from Figure 7B, the photo-response profiles of the optimal devices were both observed in the ranges of 300 to 650 nm. The obtained slightly higher J_{SC} in PBDT-DTBTT-based device was mainly benefited from its higher EQE value (larger than 40% between 350-380 and 420-600 nm). It was also worthy noted that absorption of blend and EQE response curve both exhibited an enhanced harvesting sunlight in the range of 500 to 600 nm after the conjugated plane of polymer backbone was changed from BTT to DTBTT, seen from Figures 7 and S11A. Furthermore, the integrated

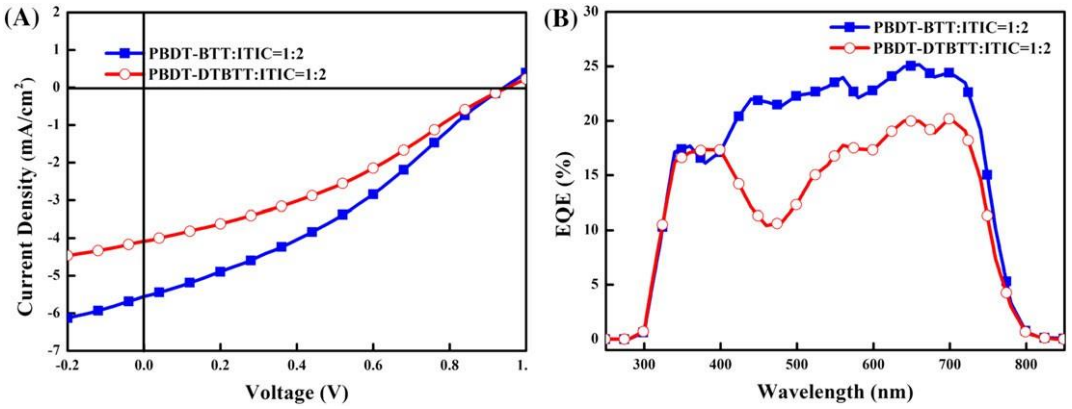

FIGURE 8 The (A) *J-V* curves and (B) external quantum efficiency (EQE) spectra of the optimized polymer solar cells (PSCs) based on polymers PBDT-BTT and PBDT-DTBTT with different weight ratio to ITIC [Colour figure can be viewed at wileyonlinelibrary.com]

TABLE 2 The optimal photovoltaic parameters of PBDT-BTT and PBDT-DTBTT

Active Layer	V_{OC} (V)	J_{SC} (mA cm^{-2})	*FF* (%)	PCE (%)
PBDT-BTT/$PC_{71}BM$ = 1:2	0.87	5.03 (4.88)	45.20	1.98
PBDT-BTT/ITIC = 1:2	0.97	5.55 (5.41)	34.63	1.76
PBDT-DTBTT/$PC_{71}BM$ = 1:1.5	0.82	6.29 (6.06)	52.45	2.73
PBDT-DTBTT/ITIC = 1:2	0.95	4.09 (3.87)	34.22	1.33

J_{SC} values from EQE curves were 6.06 and 4.88 mA cm^{-2} for the best performing PBDT-DTBTT:$PC_{71}BM$ and PBDT-BTT:$PC_{71}BM$, respectively, indicative of an error smaller than 3% in relative to J_{SC} value obtained from *J-V* curves.

3.7 | Morphology

To understand the photovoltaic properties of the resulting polymers, we investigated the morphology of blends spin coated from their CB solution by tapping-mode AFM.[42] The height and phase images of the blend film were shown in Figure 9. We can see that the root-mean-square (RMS) roughness of PBDT-BTT/$PC_{71}BM$ (1/2, *w/w*) was 0.45 nm, meanwhile RMS value for PBDT-DTBTT/$PC_{71}BM$ (1/1.5, *w/w*) films was increased to 3.82. To further investigate the real space images in the polymer-fullerene blends, the transmission electron microscopy (TEM) was further employed. As shown in Figure 10 , the PBDT-BTT/$PC_{71}BM$ and PBDT-DTBTT/$PC_{71}BM$ blend films depict large phase separation with a domain size, while one of the conjugation-enlarged PBDT-DTBTT/$PC_{71}BM$ blend film was greatly increased to approximately 200 nm. The observation from AFM and TEM both suggested that when an enlarged π-conjugated system DTBTT was introduced into the polymer backbone to replace BTT, the surface and phase separation were both increased, which was in accordance with the enhanced aggregation tendency obtained from previous TD-Abs, XRD, and DFT analyses. Regretfully, these morphology measurements never explain the reason why the PBDT-DTBTT-$PC_{71}BM$ based has a relatively higher J_{SC} and *FF*. As for polymer: ITIC system, we also investigated the morphology using AFM, as shown in Figure S13. It was found that the RMS value was increased from 2.84 to 3.42 nm when BTT unit was substituted with DTBTT onto the polymer backbone, which can partially account for the decrease[43,44] in J_{SC} (from 5.55 to 4.09 mA cm^{-2}).

3.8 | Hole mobility

The carrier charge mobility of blend films commonly affected the J_{SC} and *FF* of the related PSCs. Higher hole mobility was recognized as a good issue for an improved transport without a large photocurrent loss derived from recombination of charges.[45-47] In order to investigate the influence of introducing an extended conjugated structure into the polymer backbone on the hole mobility of the polymer, the charge-carrier mobilities of PBDT-BTT/$PC_{71}BM$ and PBDT-DTBTT/$PC_{71}BM$ films were estimated by using the SCLC theory with the

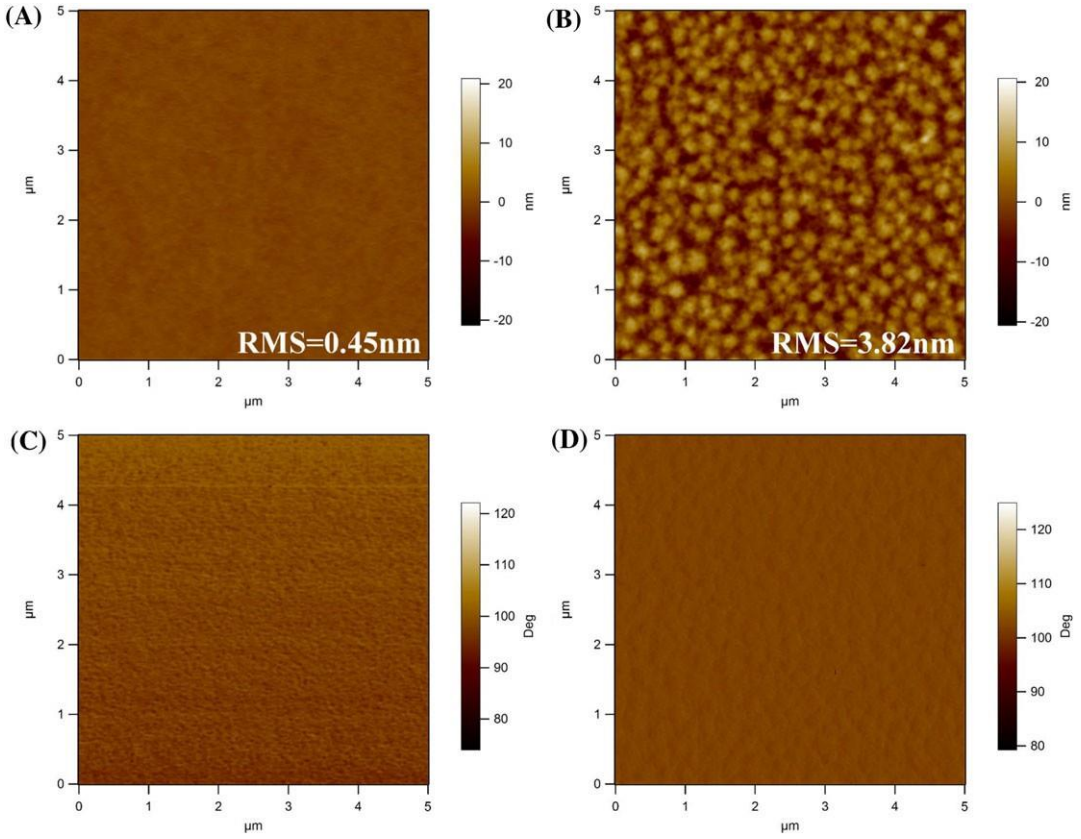

FIGURE 9 Tapping atomic force microscopy (AFM) (A,B) height images and (C,D) phase image (5 × 5 μm) for the blend films of PBDT-BTT/$PC_{71}BM$ (1:2) and PBDT-DTBTT/$PC_{71}BM$ (1:1.5) [Colour figure can be viewed at wileyonlinelibrary.com]

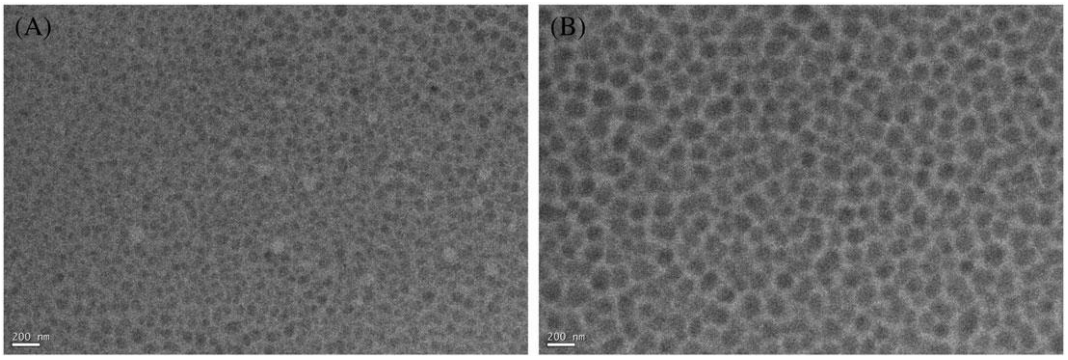

FIGURE 10 Transmission electron microscopy (TEM) topography images for the (A) blend films of PBDT-BTT/$PC_{71}BM$ (1:2) and (B) the blend films of PBDT-DTBTT/$PC_{71}BM$ (1:1.5)

device structures of ITO/PFN/active layer/MoO_3/Ag. The mobility was determined by SCLC model, which was described by Equation 1.

$$\mu \frac{8L^3 J}{9\varepsilon^0 \varepsilon V^2} \quad (1)$$

The thicknesses of the active layer materials were fixed about 98 nm (PBDT-BTT) and 103 nm (PBDT-DTBTT), respectively. The *J-V* characteristics of the devices from the PBDT-BTT and PBDT-DTBTT were presented in Figures 11 and S14, and the corresponding date was given in Table 3. The hole mobilities of PBDT-BTT and PBDT-DTBTT were calculated to about 7.28×10^{-5} and 5.90×10^{-4} cm^2 V^{-1} s^{-1}, respectively. It was exhibited that the obviously enhanced hole mobility of PBDT-DTBTT was strongly related to the more ordered molecular structure and more planar and linear molecular configuration in the previous XRD and DFT analyses, which could account for the extended conjugated PBDT-DTBTT achieving the higher J_{SC} and *FF*.

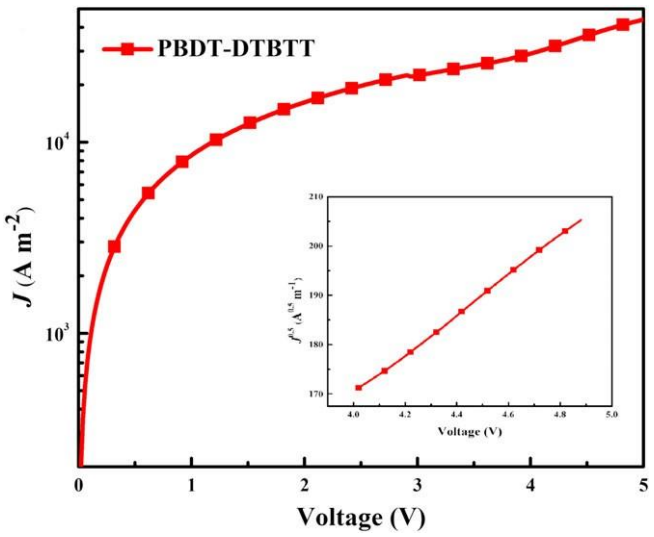

FIGURE 11 *J-V* characteristics for hole-only devices with copolymer PBDT-DTBTT shows the $J^{1/2}$-*V* curve [Colour figure can be viewed at wileyonlinelibrary.com]

TABLE 3 Hole mobilities of polymers and blend measured by space-charge limited current (SCLC) model

Active Layer	Ratios (*w:w*)	Thickness (nm)	Slope μ_h ($cm^2V^{-1}s^{-1}$)
PBDT-BTT	1:2	98	14.90 7.28×10^{-5}
PBDT-DTBTT	1:1.5	103	41.39 5.90×10^{-4}

4 | CONCLUSION

To conclude, two WBG CPs PBDT-BTT and PBDT-DTBTT have been synthesized and systematically investigated. A comprehensive comparison between PBDT-BTT and PBDT-DTBTT demonstrated that the extending of conjugated length and enlarging of conjugated planarity in DTBTT unit endowed the polymer with a wider absorption range, more ordered molecular structure, more planar and larger molecular configuration, and thus higher hole mobility in spite of raised E_{HOMO}. Even if there were more matched E_{HOMO}/E_{LUMO} and the complementary absorption with ITIC, the relatively poor photovoltaic performance was obtained, which was attributed to the lower J_{SC} and *FF*. The best photovoltaic devices exhibited that PBDT-DTBTT/$PC_{71}BM$ showed the PCE of 2.73% with J_{SC} of 6.29 mA cm^{-2} and *FF* of 52.45%, whereas control PBDT-BTT/$PC_{71}BM$ exhibited a PCE of 1.98%, with a V_{OC} of 0.87 V, J_{SC} of 5.03 mA cm^{-2}, and *FF* of 45.20%. The 38% enhanced PCE is mainly benefited from improved absorption and enhanced SCLC hole mobility after the molecular tuning of extending the conjugated system. Our results demonstrated that a strategy of an extended π-conjugated system on donor backbones was effective to tune optical electronic property and boost up the PCE in design of WBG donor materials.

ACKNOWLEDGEMENTS

The authors are deeply grateful to National Natural Science Foundation of China (51463011 and 61404067), the Natural Science Foundation of Gansu Province (no. 17JR5RA093), the Foundation of A Hundred Youth Talents Training (152022), and Excellent Team of Scientific Research in Lanzhou Jiaotong University (201705 and 201703) for financial support. We also express our thanks to Instrument Analysis Center of Lanzhou Jiaotong University for related testing support.

ORCID

Yangjun Xia https://orcid.org/0000-0002-4886-5914

REFERENCES

1. Li Y. Molecular design of photovoltaic materials for polymer solar cells: toward suitable electronic energy levels and broad absorption. *Acc Chem Res*. 2012;45(5):723-733.
2. Liu Y, Zhao J, Li Z, et al. Aggregation and morphology control enables multiple cases of high-efficiency polymer solar cells. *Nat Commun*. 2014;5(5):5293.
3. Zhao W, Li S, Yao H, et al. Molecular optimization enables over 13% efficiency in organic solar cells. *J Am Chem Soc*. 2017;139(21):7148-7151.
4. Huo L, Liu T, Sun X, Cai Y, Heeger AJ, Sun Y. Single-junction organic solar cells based on a novel wide-bandgap polymer with efficiency of 9.7%. *Adv Mater*. 2015;27(18):2938-2944.
5. Peet J, Kim JY, Coates NE, et al. Efficiency enhancement in low-bandgap polymer solar cells by processing with alkane dithiols. *Nat Mater*. 2007;6(7):497-500.
6. Tong J, Li J, Zhang P, et al. Naphtho[1,2-*c*:5,6-*c*′]bis[1,2,5]thiadiazole-based conjugated polymers consisting of oligothiophenes for efficient polymer solar cells. *Polymer*. 2017;121:183-195.
7. Lin Y, Wang J, Zhang ZG, et al. An electron acceptor challenging fullerenes for efficient polymer solar cells. *Adv Mater*. 2015;27(7):1170-1174.
8. Mei J, Bao Z. Side chain engineering in solution-processable conjugated polymers. *Chem Mater*. 2014;26(1):604-615.
9. Hou J, Park MH, Zhang S, et al. Bandgap and molecular energy level control of conjugated polymer photovoltaic materials based on benzo[1,2-*b*:4,5-*b*′]dithiophene. *Macromolecules*. 2008;41(16):6012-6018.
10. Yao H, Ye L, Zhang H, Hou J. Molecular design of benzodithiophene-based organic photovoltaic materials. *Chem Rev*. 2016;16(12):7397-7457.
11. Nielsen CB, Fraser JM, Schroeder BC, et al. Benzotrithiophene—a planar, electron-rich building block for organic semiconductors. *Org Lett*. 2011;13(9):2414-2417.
12. Zhang G, Zhu M, Guo J, et al. Benzodithiophene and benzotrithiophene-based conjugated polymers for organic thin-film transistors application: impact of conjugated- and acyl-side chain. *Org Electron*. 2014;15(10):2608-2615.
13. Nielsen CB, Ashraf RS, Schroeder BC, et al. Random benzotrithiophene-based donor-acceptor copolymers for efficient organic photovoltaic devices. *Chem Commun*. 2012;48(47):5832-5834.
14. Zhao X, Yang D, Lv H, Yin L, Yang X. New benzotrithiophene derivative with a broad band gap for high performance polymer solar cells. *Polym Chem*. 2013;4(1):57-60.
15. Zhang G, Yuan J, Li P, et al. Benzotrithiophene and benzodithiophene-based polymers for efficient polymer solar cells with high open-circuit voltage. *Polym Chem*. 2013;4(11):3390-3397.
16. Patra D, Chiang CC, Chen WA, Wei KH, Wu MC, Chu CW. Solution-processed benzotrithiophene-based donor molecules for efficient bulk heterojunction solar cells. *J Mater Chem A*. 2013;1(26):7767-7774.
17. Guo X, Puniredd SR, Baumgarten M, Pisula W, Müllen K. Benzotrithiophene-based donor-acceptor copolymers with distinct supramolecular organizations. *J Am Chem Soc*. 2012;134(20):8404-8407.
18. Wang J, Yin P, Wu Y, Liu G, Cui C, Shen P. Synthesis and optoelectronic property manipulation of conjugated polymer photovoltaic materials based on benzo[*d*]dithieno[3,2-*b*;2′,3′-*f*]azepine. *Polymer*. 2018;147:184-195.
19. Son HJ, Lu L, Chen W, et al. Synthesis and photovoltaic effect in dithieno[2,3-*d*:2′,3′-*d*′]benzo[1,2-*b*:4,5-*b*′]dithiophene-based conjugated polymers. *Adv Mater*. 2013;25(6):838-843.
20. Liu H, Zhang Z, Huang M, Zhao B, Zhang J, Tan S. A trilobal non-fullerene electron acceptor based on benzo[1,2-*b*:3,4-*b*′:5,6-*b*′]trithiophene and perylenediimide for polymer solar cells. *Synth Met*. 2017;227:122-130.
21. Han J, Qi J, Zheng X, et al. Low-bandgap donor-acceptor polymers for photodetectors with photoresponsivity from 300 nm to 1600 nm. *J Mater Chem C*. 2017;5(1):159-165.
22. Tong J, An L, Lv J, et al. Enhanced photovoltaic performance in D-π-A copolymers containing triisopropylsilylethynyl-substituted dithienobenzodithiophene by modulating the electron-deficient units. *Polymers*. 2019;11:12.
23. Wu Y, Li Z, Ma W, et al. PDT-S-T: a new polymer with optimized molecular conformation for controlled aggregation and π-π stacking and its application in efficient photovoltaic devices. *Adv Mater*. 2013;25(25):3449-3455.
24. Qi F, Zhang Y, Wan M, Liu J, Huo L. Enhanced photovoltaic performance of polymer solar cells through design of a fused dithienosilolodithiophene structure with an enlarged π-conjugated system. *J Mater Chem C*. 2018;6(15):4208-4216.
25. Tong J, An L, Li J, et al. Effects of alkyl side chain length of low bandgap naphtho[1,2-*c*:5,6-*c*′]bis[1,2,5]thiadiazole-based copolymers on the optoelectronic properties of polymer solar cells. *J Polym Sci A Polym Chem*. 2018;56(18):2059-2071.
26. Wang E, Hou L, Wang Z, et al. Side-chain architectures of 2,7-carbazole and quinoxaline-based polymers for efficient polymer solar cells. *Macromolecules*. 2011;44(7):2067-2073.
27. Huo L, Zhou Y, Li Y. Alkylthio-substituted polythiophene: absorption and photovoltaic properties. *Macromol Rapid Commun*. 2009;30(11):925-931.
28. Chen H-Y, Hou J, Zhang S, et al. Polymer solar cells with enhanced open-circuit voltage and efficiency. *Nat Photonics*. 2009;3(11):649-653.
29. Gao P, Tong J, Guo P, et al. Medium band gap conjugated polymers from thienoacene derivatives and pentacyclic aromatic lactam as promising alternatives of poly(3-hexylthiophene) in photovoltaic application. *J Polym Sci A Polym Chem*. 2018;56(1):85-95.
30. Huang F, Wu H, Wang D, Yang W, Cao Y. Novel electroluminescent conjugated polyelectrolytes based on polyfluorene. *Chem Mater*. 2004;16(4):708-716.
31. An M, Xie F, Geng X, et al. A high-performance D-A copolymer based on dithieno[3,2-*b*:2,3-*d*]pyridin-5(4H)-one unit compatible with fullerene and nonfullerene acceptors in solar cells. *Adv Energy Mater*. 2017;7(14):1602509.
32. Blouin N, Michaud A, Leclerc M. A low-bandgap poly(2,7-carbazole) derivative for use in high-performance solar cells. *Adv Mater*. 2010;19(17):2295-2300.
33. Wang M, Hu X, Liu P, et al. Donor-acceptor conjugated polymer based on naphtho[1,2-*c*:5,6-*c*]bis[1,2,5]thiadiazole for high-performance polymer solar cells. *J Am Chem Soc*. 2011;133(25):9638-9641.
34. Hu H, Jiang K, Kim JH, et al. Influence of fluorination on the properties and performance of isoindigo-quaterthiophene-based polymers. *J Mater Chem A*. 2016;4(14):5039-5043.
35. Chen J, Duan L, Xiao M, et al. Tuning the central fused ring and terminal units to improve the photovoltaic performance of Ar(A-D)$_2$ type small molecules in solution-processed organic solar cells. *J Mater Chem A*. 2016;4(13):4952-4961.
36. Pommerehne J, Vestweber H, Guss W, et al. Efficient two layer LEDs on a polymer blend basis. *Adv Mater*. 2010;7(6):551-554.

37. Shin N, Yun HJ, Yoon Y, et al. Highly stable polymer solar cells based on poly(dithienobenzodithiophene-*co*-thienothiophene). *Macromolecules*. 2015;48(12):3890-3899.

38. Wang J, Xiao M, Chen W, et al. Extending π-conjugation system with benzene: an effective method to improve the properties of benzodithiophene-based polymer for highly efficient organic solar cells. *Macromolecules*. 2014;47(22):7823-7830.

39. Frisch MJ, Trucks GW, Schlegel HB, et al. Gaussian 09, Gaussian, Inc, Wallingford, CT, USA, 2009.

40. He Z, Zhong C, Su S, Xu M, Wu H, Cao H. Enhanced power-conversion efficiency in polymer solar cells using an inverted device structure. *Nat Photonics*. 2012;6(9):593-597.

41. Wienk MM, Kroon JM, Verhees WJ, et al. Efficient methano[70]-fullerene/MDMO-PPV bulk heterojunction photovoltaic cells. *Angew Chem*. 2010;42(29):3371-3375.

42. Yuan J, Xiao L, Liu B, et al. New alkoxylphenyl substituted benzo[1,2-*b*:4,5-bprime]dithiophene-based polymers: synthesis and application in solar cells. *J Am Chem Soc*. 2013;1(36):10639-10645.

43. Xiao L, Yuan J, Zou Y, et al. A new polymer from fluorinated benzothiadiazole and alkoxylphenyl substituted benzo[1,2-*b*:4,5-*b*] dithiophene: synthesis and photovoltaic applications. *Synth Met*. 2014;187:201-208.

44. Lou SJ, Szarko JM, Xu T, Yu L, Marks TJ, Chen LX. Effects of additives on the morphology of solution phase aggregates formed by active layer components of high-efficiency organic solar cells. *J Am Chem Soc*. 2011;133(51):20661-20663.

45. Wang Z, Li Z, Liu J, et al. Solution-processable small molecules for high-performance organic solar cells with rigidly fluorinated 2,2'-bithiophene central cores. *ACS Appl Mater Interfaces*. 2016;8(18):11639-11648.

46. Li J, Liang Z, Wang Y, et al. Enhanced efficiency of polymer solar cells through synergistic optimization of mobility and tuning donor alloys by adding high-mobility conjugated polymers. *J Mater Chem C*. 2018;6(41):11015-11022.

47. Koster LJA, Mihailetchi VD, Blom PWM. Bimolecular recombination in polymer/fullerene bulk heterojunction solar cells. *Appl Phys Lett*. 2006;88(5):052104.

SUPPORTING INFORMATION

Additional supporting information may be found online in the Supporting Information section at the end of the article.

How to cite this article: Zhang X, Zhang M, Tong J, et al. Synthesis and photovoltaic investigation of dithieno[2,3-*d*:2′,3′-*d*′]-benzo[1,2-*b*:3,4-*b*′:5,6-*d*″]trithiophene-based conjugated polymer with an enlarged π-conjugated system. *Polym Adv Technol*. 2019;30:1290-1302. https://doi.org/10.1002/pat.4562